

Ferromagnetism and Nonmetallic Transport of Thin-Film α -FeSi₂: A Stabilized Metastable Material

Guixin Cao,¹ D. J. Singh,² X.-G. Zhang,¹ German Samolyuk,² Liang Qiao,¹ Chad Parish,² Ke Jin,³ Yanwen Zhang,^{3,2} Hangwen Guo,² Siwei Tang,^{1,3} Wenbin Wang,² Jieyu Yi,^{1,3} Claudia Cantoni,² Wolter Siemons,² E. Andrew Payzant,¹ Michael Biegalski,¹ T. Z. Ward,² David Mandrus,^{3,2} G. M. Stocks,² and Zheng Gai^{1,*}

¹Center for Nanophase Materials Sciences, Oak Ridge National Laboratory, Oak Ridge, Tennessee 37831, USA

²Materials Science and Technology Division, Oak Ridge National Laboratory, Oak Ridge, Tennessee 37831-6056, USA

³Department of Materials Science and Engineering, University of Tennessee, Knoxville, Tennessee 37996, USA

(Received 1 September 2014; revised manuscript received 27 January 2015; published 7 April 2015)

A metastable phase α -FeSi₂ was epitaxially stabilized on a silicon substrate using pulsed laser deposition. Nonmetallic and ferromagnetic behaviors are tailored on α -FeSi₂ (111) thin films, while the bulk material of α -FeSi₂ is metallic and nonmagnetic. The transport property of the films renders two different conducting states with a strong crossover at 50 K, which is accompanied by the onset of a ferromagnetic transition as well as a substantial magnetoresistance. These experimental results are discussed in terms of the unusual electronic structure of α -FeSi₂ obtained within density functional calculations and Boltzmann transport calculations with and without strain. Our finding sheds light on achieving ferromagnetic semiconductors through both their structure and doping tailoring, and provides an example of a tailored material with rich functionalities for both basic research and practical applications.

DOI: 10.1103/PhysRevLett.114.147202

PACS numbers: 75.47.Np, 68.55.-a, 72.80.Ga

Transition-metal disilicides have been extensively investigated in bulk and thin film forms for their roles as constituents in microelectronic and optoelectronic devices [1–5]. In contrast to other metallic disilicides, environmentally friendly iron disilicide (FeSi₂) is particularly appealing as a material for thermoelectric or optoelectronic devices due to its semiconductor behavior [3–5]. Very recently, it has been theoretically predicted that semiconducting iron disilicide can even become magnetic through a low level of doping [6]. FeSi₂ possesses two main phases: i.e., an α phase and a β phase. While β -FeSi₂ is a well-studied room temperature stable orthorhombic phase, α -FeSi₂ is a metastable tetragonal phase with the fluorite structure, which only exists at temperatures above 950 °C [3–5,7–9]. During cooling, the high temperature stable α -FeSi₂ phase transforms into the β -FeSi₂ phase in terms of an energy-lowering Jahn-Teller-like distortion, accompanied by a spontaneous metal-semiconductor transition [10–12]. Although the impure α phase (nonmagnetic) can only be occasionally obtained via facing-target sputtering [13], ion implantation [14], and the annealing of a few monolayer films of Fe on Si(111) [15,16] and Si(001) [17,18] substrates, it already shows interesting applications as electrodes or an interconnecting material, precursors for achieving Si- β heterostructures [15,19]. Physically, the magnetic properties of metastable phases can be drastically different from those of equilibrium phases [20,21]. Moreover, special heteroepitaxial relationships can induce new properties and changes of the band structure [2]. The stabilization of the pure metastable α phase is not only important for material applications but also for providing

a prototypical system to understand the interplay between chemical bonding and the electronic [22] and magnetic properties [19,20].

Here, we report the epitaxially stabilized metastable phase of α -FeSi₂ (111) thin films grown on a Si(001) substrate [α -FeSi₂(111)||Si(001)] via pulsed laser deposition. New electronic behavior, which is in between that of metals and semiconductors, as well as ferromagnetism are tailored in the film although the α -FeSi₂ phase is thought to be metallic and nonmagnetic. An unusual transport property with a strong crossover at 50 K was found accompanied by the onset of ferromagnetism with a first order transition, as well as a substantial magnetoresistance. Density functional theory (DFT) calculations were performed to provide a framework for understanding the transport property and to verify the ferromagnetism with a slight excess of Fe in stoichiometry. The stabilizing and tailoring of the metastable metallic phase towards a semiconducting and magnetic phase may open new pathways to potential device applications.

α -FeSi₂(111)||Si(001) films were grown in an ultrahigh vacuum pulsed laser deposition system with reflection high-energy electron diffraction (RHEED). The Si(001) substrate was processed until it showed a sharp RHEED pattern [Fig. 1(a)]. The films were grown at 754 °C with a laser flux of 1.2 J cm⁻² at 2 Hz. During the deposition, the RHEED pattern changed rapidly from Si(001)-(2 × 1) to a new set of patterns as shown in Fig. 1(a), then remained the same to the end of the growth. The film thickness of 50 nm was determined using a profilometer and AFM. The structural properties were investigated by high-resolution

x-ray diffraction and electron backscatter diffraction. The magnetic properties were measured on a Quantum Design magnetic property measurement system under fields up to 7 T. The electrical resistivity measurements were performed using a Quantum Design physical property measurements system. The iron stoichiometry was checked using Rutherford backscattering spectrometry (RBS). A value of Fe rich around 5% was estimated from the RBS results. The RBS concentrations for other films grown at a similar growth condition are consistent.

DFT calculations were performed using the generalized gradient approximation of Perdew, Burke, and Ernzerhof [23]. These were done with the general potential linearized augmented plane wave (LAPW) method, [24] implemented in the WIEN2K code [25]. The calculations were done for the strained film without including the substrate. The LAPW sphere radii were 2.25 and 1.90 bohr for Fe and Si, respectively. The high convergence criterion was $R_{\text{MIN}}K_{\text{MAX}} = 8$, where R_{MIN} is the Si sphere radius. This yields an effective value above 9 for Fe. The standard LAPW method with added local orbitals LAPW + lo [26] was used, rather than the APW + lo method [27]. With the above parameter choice, the standard LAPW + lo basis for all momentum channels is more efficient than a mixture. Local orbitals were used both to include the $3p$ semicore state of Fe with the valence states and to relax any linearization errors in the Fe $3d$ states. The spin-orbital coupling of Fe and Si is included in the calculation. The $P4/mmm$ unit cell contains Fe at $(0, 0, 0)$ and Si at $(1/2, 1/2, \pm z)$; the value of z (0.2731) is determined by total energy minimization. With this structure, each Fe is coordinated by eight Si atoms at a distance of 2.364 Å, while each Si has a short bond to a neighboring Si at 2.333 Å, four Fe neighbors at 2.364 Å, four Si neighbors at 2.690 Å, and one elongated bond Si neighbor at 2.807 Å. The electronic potential is approximated by a hybrid atomic-sphere-approximation muffin tin with cell shape corrections [28].

Figure 1(b) shows the room temperature θ - 2θ scan of an α -FeSi₂(111)||Si(001) film. The (111) peak of α -FeSi₂ is the only extra peak observed other than the Si (002) and (004) reflections, evidencing a single crystalline tetragonal α -FeSi₂ phase with the (111) orientation. To confirm the preferred orientation of (111), and to determine the epitaxial relationship between the film and the substrate, an in-plane pole figure scan was conducted across the (202) Bragg peak of Si(001). Figure 1(c) shows the (102) Bragg peak of the (111)-type domain of the α -FeSi₂ film, which indicates that the α -FeSi₂ (102) plane is parallel to the Si (202) plane. Moreover, the (102) peak was shown in a fourfold symmetry. An electron backscatter diffraction investigation reveals a tetragonal structure with two main FeSi₂ domains of the film, confirming the high quality epitaxial nature of the films. The side view and top view of the α -FeSi₂ with the truncated (111) plane are shown in

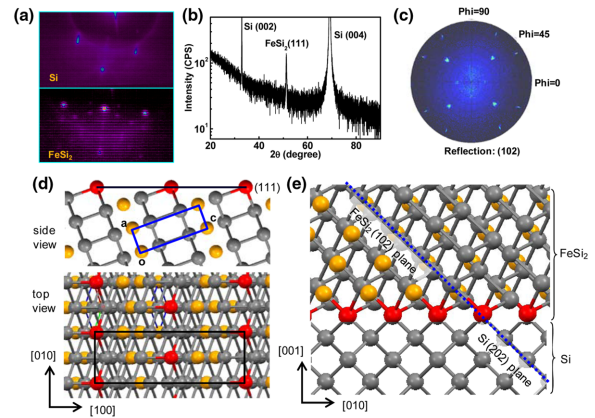


FIG. 1 (color online). (a) The RHEED patterns recorded before and after the growth of α -FeSi₂(111)||Si(001). (b) High-resolution x-ray diffraction (θ - 2θ) scan of the film. (c) The pole figure at the Si (202) plane. (d) Side view and top view of the α -FeSi₂ film with the (111) plane truncated. (e) The epitaxial relation model between the α -FeSi₂ film and Si(001)-(3 × 1).

Fig. 1(d). Each bulk α -FeSi₂ unit cell is formed by two Si atoms (gray or red) and one Fe atom (orange), outlined in blue in the side view figure. As the (111) plane is very complicated, for better viewing of the (111) unit cell, red balls are used to mark the topmost layer of the (111) surface. The (111) unit cell is outlined with a black rectangle (10.95×3.8 Å), very close to the Si(001)-(3 × 1) (11.5×3.84 Å). Based on above results, we proposed a possible epitaxial model in Fig. 1(e) that satisfies the registration of the α -FeSi₂(111) rectangular unit cell to Si(001)-(3 × 1), and the parallel relation between α -FeSi₂(102) and the Si (202) planes [marked with the dotted blue line in Fig. 1(e)].

The structure of the α -FeSi₂(111)||Si(001) film was further studied as a function of temperature T using x-ray diffraction (20 to 300 K). The T dependent d spacing was obtained from the shift of the FeSi₂(111) peak during cooling [Fig. 2(a)]. The continuous evolution of the d spacing suggests the absence of structural phase transitions versus T . The linear thermal expansion coefficient α , defined as $\alpha = (1/d)(\Delta d/\Delta T)$, is shown in Fig. 2(a). α is almost a constant at high temperature, and then decreases exponentially in a low temperature region, associated with a sign change at around 50 K.

Figure 2(b) shows the temperature dependent conductance of the α -FeSi₂(111)||Si(001) film, $\sigma(T)$, under different magnetic fields. For comparison, the counterpart of the Si substrate is also shown. It is clearly seen that the conductance of the α -FeSi₂(111)||Si(001) film gradually decreases with decreasing temperature (nonmetallic behavior), with a different trend from that of Si. Interestingly, the $\sigma(T)$ curves show an obvious slope change around 50 K. This differs drastically from the bulk phase of the material in which the conductivity shows no temperature dependence [9]. Furthermore, the conductance of the thin film

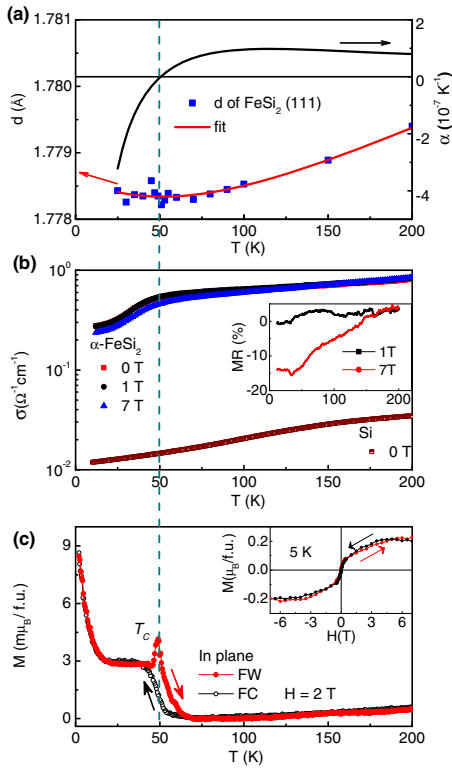


FIG. 2 (color online). (a) Temperature dependent d spacing of the (111) reflection (left y axis) and calculated α (right y axis). The red line is the polynomial fit to the experimental d spacing. α crosses zero around 50 K. (b) $\sigma(T)$ for 50 nm α -FeSi₂ (111) films under different fields and $\sigma(T)$ of Si(001). Inset shows the MR. (c) $M(T)$ curves under 2 T. The inset shows a typical $M(H)$ loop at 5 K. The dotted line around 50 K is a guide to the eye for the 50 K transitions.

shows a magnetic field dependence. The magnetoresistance (MR), $\Delta R/R = [R(0) - R(H)]/R(H)$ reaches 15% at 7 T at low temperature as shown in the inset of Fig. 2(b); the value is well beyond typical anisotropy induced magnetoresistance.

The field-cooled and field-warmed magnetization $M(T)$ of the FeSi₂ (111) film undergoes a ferromagnetic transition at 50 K [Fig. 2(c)]. The system has a first order transition indicated by a sharp cusp in magnetization around T_c . A similar feature exists for both in-plane and out-of-plane magnetization, with a stronger in-plane signal than that out of plane. The increase of the susceptibility below 10 K is attributed to an impurity induced Curie-like paramagnetic contribution. The field dependent magnetization at 5 K is shown in the inset of Fig. 2(c). The magnetization increases rapidly at low fields and saturates around 4 T as expected for ferromagnetic behavior. The magnetic saturation moment at 5 K is around $0.2 \mu_B$ per formula unit.

The MR and the coincidence of the sign change of α , crossover of the electronic transport, and magnetic transition at the same temperature of 50 K are worth further discussion. For the MR behavior, one possible explanation

is the coexistence of ferromagnetic and nonmagnetic phases. If the ferromagnetic phase has highly spin polarized transport, similar to manganites or half metals, a strong MR can be expected. This can be understood based on the calculated band structure. As discussed below in detail, there shows a strong energy dependence of the electronic structure near the Fermi energy E_F , and in particular the onset of a high density of states (DOS) just above E_F . An exchange splitting of this density of states would lead to majority spin transport, reflecting the high density of states electronic structure above the paramagnetic E_F , and the minority spin transport based on the electronic states that occur below E_F in the paramagnetic case.

There have been prior band structure calculations for α -FeSi₂; it consists of hybridized d bands on top of a Si sp band structure [10,12,29–31]. There is a large peak in the electronic DOS just above E_F , which derives from a single Fe d band (twofold degenerate with spin-orbit interaction), with different calculations differing about the exact position of the onset relative to E_F . The nominal d occupancy is 8, as in elemental Fe, implying that Fe is not a dopant in this material. As such, the Fermi energy position is expected to be insensitive to the Fe stoichiometry, although the DOS may broaden due to disorder effects in actual samples.

To understand the abnormal transport and ferromagnetism tailored in our strain stabilized α -FeSi₂(111)||Si(001) films, the calculated band structure and DOS for both the paramagnetic and ferromagnetic phase as well as the majority and minority spin states of Fe and substitutional Fe in strained structures for α -FeSi₂ using DFT are shown in Figs. 3(a) and 3(b). The distinct dip in the DOS is consistent with recent work [32]. Importantly, in our calculation the onset of the DOS peak is almost exactly at the Fermi energy, yielding a highly asymmetric DOS around E_F . This peak comes from the flat band around the zone boundary at $k_z = 0$, i.e., the band seen just at E_F along X - M line in Fig. 3(a). This band has antibonding Fe d_{z^2} -Si sp character. The other band that crosses E_F has $d_{x^2-y^2}$ character. The strongest predicted signature of this strong energy dependence is a large negative thermopower, unusual for a metal. This prediction provides a test of the electronic structure. One may expect two effects from this electronic structure. The first is that if it becomes ferromagnetic, the transport will be substantially spin polarized, which would be reflected in a negative magnetoresistance, as seen in the inset of Fig. 2(b). Second, in nonmagnetic samples, which have been reported to grow under other conditions, a temperature dependent crossover in transport may be expected, specifically from a low density of states metal to an effectively higher density of states metal with increasing T .

The origin of the ferromagnetism of the α -FeSi₂ thin films was investigated using the local density approximation of the DFT implemented within the layer-KKR code [33] and coherent-potential approximation [34] to treat substitutional

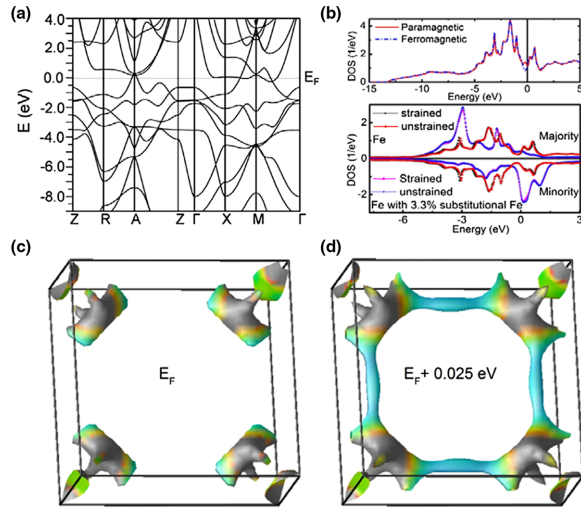


FIG. 3 (color online). (a) Calculated band structure of α -FeSi₂, including the spin-orbit interaction. (b) Top panel: total DOS for paramagnetic and ferromagnetic phases with the Si sites containing 3.3% substitutional Fe. Bottom panel: majority and minority spin states of Fe and substitutional Fe in strained structures, respectively. (c),(d) Fermi surface of α -FeSi₂ with E_F and $E_F + 0.025$ eV. In these plots Γ is at the center.

disorder as shown in Fig. 3(b). The calculations were done using both the experimentally measured strained ($a = 2.69$ Å, $c = 5.14$ Å) and the unstrained ($a = 2.72$ Å, $c = 5.42$ Å) lattice parameters. For the strained lattice, we found that as a small percentage of Si atoms are substituted by Fe those Fe atoms maintain a nearly constant moment of $2.38 \mu_B$ per Fe. Meanwhile, the Fe atoms on the Fe sublattice also acquire a small moment proportional to the amount of substitutional Fe atoms on the Si sublattice, as shown in the bottom panel of Fig. 3(b). When the substitutional Fe concentration reaches 3.3% (or 6.6% excess per Fe atom), the total net moment reaches $0.2 \mu_B$ per unit cell, consistent with the experimental moment [in the inset of Fig. 2(c)]. The total energy of the ferromagnetic phase is lower than that of the paramagnetic phase by about 8.66 meV per unit cell. For the unstrained lattice, the energies are reversed, with the total energy of the paramagnetic phase lower by about 7.23 meV per unit cell.

The Fermi surfaces for E_F and $E_F + 0.025$ eV within a rigid band model are shown in Figs. 3(c) and 3(d). The topology of the Fermi surfaces dramatically changes on such a low energy scale. For the actual E_F the Fermi surface consists of small compensating pockets. These include a hole surface around the M point, an electron sheet, and a complex sheet along the Γ - M line. This complex sheet forms connections near but not exactly at the zone boundary as the Fermi energy is raised. The resulting pipes are a quasi-two-dimensional structure and are the origin of the sharp rise in the DOS. This is reminiscent of the structure seen in p -type PbTe [35] and, as in that case, it is expected to affect the transport properties. Qualitatively,

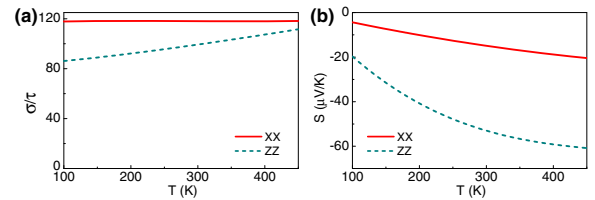


FIG. 4 (color online). (a) σ/τ (arbitrary units) versus T . (b) $S(T)$ of α -FeSi₂ within the constant scattering time approximation.

what may be expected is that the effective DOS will increase with T , while the Fermi energy will be pushed down. The conductivity at low T can be written as $\sigma \propto N(E_F) \langle v_F^2 \rangle \tau$, for finite T , see Ref. [36]. Here τ is an inverse scattering rate, and $(\langle v_F^2 \rangle)^{1/2}$ is the effective average Fermi velocity in the direction of the conductivity. $\sigma(T)$ comes from the product of a band structure dependent term $N(E_F)$ and the scattering term τ . For the former term, the T dependence comes from broadening with a derivative of the Fermi function, while the scattering term in general has a complex T dependence depending on the scattering mechanism, typically electron-phonon and electron-spin-fluctuation interactions in metals at moderate temperatures. In the present case, both terms are expected to be nontrivial.

In order to examine this further, we performed calculations of transport functions σ/τ [Fig. 4(a)] within Boltzmann transport theory [36,37]. In a metal, σ/τ has negligible T dependence. Here, however, we find a substantial T dependence for c -axis transport because of the structure in the DOS near E_F . At low T , the scattering τ will be governed by point defects and is expected to reflect the behavior of a moderate $N(E_F)$, three-dimensional metal with disorder. However, as T increases, the effective $N(E_F)$ increases as discussed above. Qualitatively, this should both open additional scattering channels for phase space reasons and also may lead to additional scattering if the increased $N(E_F)$ brings the system closer to lattice instabilities or magnetism. Although our calculation does not quantify the transport, the nonmetallic and complicated transport behaviors of the thin films are qualitatively understood. It is noted that the resistance decreases with temperature, but in a nonactivated manner, as shown in Fig. 2(b). We attribute the resistance to extrinsic grain and domain boundary resistance in the film, consistent with the magnetoresistance.

Interestingly, we also find an anisotropic Seebeck coefficient $S(T)$ that is anomalously large for a metal especially in the c -axis direction, as displayed in Fig. 4(b). $S(T)$ is negative (n type) for both in-plane and c -axis transport, but is much larger in magnitude for the c -axis direction. This reflects the d_{z^2} character of the flat band, which leads to a faster relative increase of the conductivity with energy for the c -axis direction [note that at low T according to the Mott formula $S(T)/T \propto (d\sigma/dE)/\sigma$].

Overall, $S(T)$ is more anisotropic than σ/τ , which is also unusual [38] and will be confirmed by further experiments.

In summary, the unusual transport behavior and a temperature dependent crossover in the transport and magnetic properties of α -FeSi₂ (111) thin films were tailored by both strain stabilization and substitutional Fe atoms on the Si sublattice. The results were explained based on the fine details of the electronic structure, the stoichiometry, and the strained structure of the film. The material provides an example of a stabilized pure phase with rather interesting physical properties for both basic scientific research and practical applications in, for example, achieving ferromagnetic semiconductors.

This research was conducted at the Center for Nanophase Materials Sciences, which is sponsored at Oak Ridge National Laboratory by the Scientific User Facilities Division, Office of Basic Energy Sciences (Z. G., G. C., X.-G. Z., L. Q., M. B., E. A. P.), U.S. Department of Energy. Part of this effort was supported by the U.S. DOE, Office of Basic Energy Sciences, Materials Sciences and Engineering Division (D. J. S., G. M. S., T. Z. W., G. M. S., Y. Z., C. P.), and under U.S. DOE Grant No. DE-SC0002136 (H. G., W. W.).

*Corresponding author.
gaiz@ornl.gov

- [1] D. Shah, D. Berczik, D. Anton, and R. Hecht, Appraisal of other silicides as structural materials, *Mater. Sci. Eng. A* **155**, 45 (1992).
- [2] K. Yamaguchi and K. Mizushima, Luminescent FeSi₂ Crystal Structures Induced by Heteroepitaxial Stress on Si(111), *Phys. Rev. Lett.* **86**, 6006 (2001).
- [3] D. Leong, M. Harry, K. Reeson, and K. Homewood, A silicon/iron-disilicide light-emitting diode operating at a wavelength of 1.5 μm , *Nature (London)* **387**, 686 (1997).
- [4] B. Egert and G. Panzner, Bonding state of silicon segregated to α -iron surfaces and on iron silicide surfaces studied by electron spectroscopy, *Phys. Rev. B* **29**, 2091 (1984).
- [5] M. Seibt, R. Khalil, V. Kveder, and W. Schröter, Electronic states at dislocations and metal silicide precipitates in crystalline silicon and their role in solar cell materials, *Appl. Phys. A* **96**, 235 (2009).
- [6] D. J. Singh and D. Parker, Itinerant magnetism in doped semiconducting β -FeSi₂ and CrSi₂, *Sci. Rep.* **3**, 3517 (2013).
- [7] A. Cullis and L. Katz, Electron microscope study of electrically active impurity precipitate defects in silicon, *Philos. Mag.* **30**, 1419 (1974).
- [8] C. Kloc, E. Arushanov, M. Wendl, H. Hohl, U. Malang, and E. Bucher, Preparation and properties of FeSi, α -FeSi₂ and β -FeSi₂ single crystals, *J. Alloys Compd.* **219**, 93 (1995).
- [9] T. Hirano and M. Kaise, Electrical resistivities of single-crystalline transition-metal disilicides, *J. Appl. Phys.* **68**, 627 (1990).
- [10] R. Girlanda, E. Piparo, and A. Balzarotti, Band structure and electronic properties of FeSi and α -FeSi₂, *J. Appl. Phys.* **76**, 2837 (1994).
- [11] N. E. Christensen, Electronic structure of β -FeSi₂, *Phys. Rev. B* **42**, 7148 (1990).
- [12] S. Eisebitt, J.-E. Rubensson, M. Nicodemus, T. Böske, S. Blügel, W. Eberhardt, K. Radermacher, S. Mantl, and G. Bihlmayer, Electronic structure of buried α -FeSi₂ and β -FeSi₂ layers: Soft-x-ray-emission and -absorption studies compared to band-structure calculations, *Phys. Rev. B* **50**, 18330 (1994).
- [13] S. Pan, C. Ye, X. Teng, H. Fan, and G. Li, Controllable growth of α - and β -FeSi₂ thin films on Si(100) by facing-target sputtering, *Phys. Status Solidi A* **204**, 3316 (2007).
- [14] X. Lin, M. Behar, J. Desimoni, H. Bernas, J. Washburn, and Z. Liliental-Weber, Low-temperature ion-induced epitaxial growth of α -FeSi₂ and cubic FeSi₂ in Si, *Appl. Phys. Lett.* **63**, 105 (1993).
- [15] N. Jedrecy, A. Waldhauer, M. Sauvage-Simkin, R. Pinchaux, and Y. Zheng, Structural characterization of epitaxial α -derived FeSi₂ on Si(111), *Phys. Rev. B* **49**, 4725 (1994).
- [16] J. Chevrier, P. Stocker, L. Vinh, J. Gay, and J. Derrien, Epitaxial Growth of α -FeSi₂ on Si(111) at Low Temperature, *Europhys. Lett.* **22**, 449 (1993).
- [17] F. Maeda, H. Hibino, S. Suzuki, and F. Z. Guo, Oxide-mediated formation of α -FeSi₂ on Si(001) studied by X-ray adsorption near edge structure analysis using SPELEEM, *Surf. Interface Anal.* **40**, 1747 (2008).
- [18] C. Detavernier, C. Lavoie, J. Jordan-Sweet, and A. S. Özcan, Texture of tetragonal α -FeSi₂ films on Si(001), *Phys. Rev. B* **69**, 174106 (2004).
- [19] J. Tripathi, M. Garbrecht, W. Kaplan, G. Markovich, and I. Goldfarb, The effect of Fe-coverage on the structure, morphology and magnetic properties of α -FeSi₂ nanoislands, *Nanotechnology* **23**, 495603 (2012).
- [20] J. Shen, Z. Gai, and J. Kirschner, Growth and magnetism of metallic thin films and multilayers by pulsed-laser deposition, *Surf. Sci. Rep.* **52**, 163 (2004).
- [21] M. van Schilfgaarde, I. Abrikosov, and B. Johansson, Origin of the Invar effect in iron-nickel alloys, *Nature (London)* **400**, 46 (1999).
- [22] J. Haeni *et al.*, Room-temperature ferroelectricity in strained SrTiO₃, *Nature (London)* **430**, 758 (2004).
- [23] J. P. Perdew, K. Burke, and M. Ernzerhof, Generalized Gradient Approximation Made Simple, *Phys. Rev. Lett.* **77**, 3865 (1996).
- [24] L. Nordstrom and D. J. Singh, *Planewaves, pseudopotentials, and the LAPW method* (Springer, New York, 2006).
- [25] P. Blaha, K. Schwarz, G. Madsen, D. Kvasnicka, and J. Luitz, *WIEN2k: An augmented plane wave plus local orbitals program for calculating crystal properties* (Vienna University of Technology, Vienna, Austria, 2001).
- [26] D. Singh, Ground-state properties of lanthanum: Treatment of extended-core states, *Phys. Rev. B* **43**, 6388 (1991).
- [27] E. Sjöstedt, L. Nordström, and D. Singh, An alternative way of linearizing the augmented plane-wave method, *Solid State Commun.* **114**, 15 (2000).

- [28] X.-G. Zhang and D. M. C. Nicholson, Generalized local-density approximation for spherical potentials, *Phys. Rev. B* **60**, 4551 (1999).
- [29] J. van Ek, P. E. A. Turchi, and P. A. Sterne, Fe, Ru, and Os disilicides: Electronic structure of ordered compounds, *Phys. Rev. B* **54**, 7897 (1996).
- [30] Y. Imai, M. Mukaida, and T. Tsunoda, Comparison of density of states of transition metal disilicides and their related compounds systematically calculated by a first-principle pseudopotential method using plane-wave basis, *Intermetallics* **8**, 381 (2000).
- [31] Y. Imai, M. Mukaida, and T. Tsunoda, Calculation of electronic energy and density of state of iron-disilicides using a total-energy pseudopotential method, *CASTEP, Thin Solid Films* **381**, 176 (2001).
- [32] W. Müller, J. Tomczak, J. Simonson, G. Smith, G. Kotliar, and M. Aronson, Protected Fe valence in quasi-two dimensional α -FeSi₂, [arXiv:1408.3606](https://arxiv.org/abs/1408.3606).
- [33] J. M. MacLaren, S. Crampin, D. D. Vvedensky, and J. B. Pendry, Layer Korringa-Kohn-Rostoker technique for surface and interface electronic properties, *Phys. Rev. B* **40**, 12164 (1989).
- [34] J. S. Faulkner and G. M. Stocks, Calculating properties with the coherent-potential approximation, *Phys. Rev. B* **21**, 3222 (1980).
- [35] D. Parker, X. Chen, and D. J. Singh, High Three-Dimensional Thermoelectric Performance from Low-Dimensional Bands, *Phys. Rev. Lett.* **110**, 146601 (2013).
- [36] G. K. H. Madsen, K. Schwarz, P. Blaha, and D. J. Singh, Electronic structure and transport in type-I and type-VIII clathrates containing strontium, barium, and europium, *Phys. Rev. B* **68**, 125212 (2003).
- [37] G. K. H. Madsen and D. J. Singh, BoltzTraP. A code for calculating band-structure dependent quantities, *Comput. Phys. Commun.* **175**, 67 (2006).
- [38] K. P. Ong, D. J. Singh, and P. Wu, Unusual Transport and Strongly Anisotropic Thermopower in PtCoO₂ and PdCoO₂, *Phys. Rev. Lett.* **104**, 176601 (2010).